Growth of glass-embedded Cu nanoparticles: A low-frequency Raman scattering study

S. Sirotkin,[1] E. Cottancin,[2] L. Saviot,[3] E. Bernstein,[4] and A. Mermet[1]

[1]*Laboratoire de Physico-Chimie des Matériaux Luminescents, Université de Lyon, Université Claude Bernard Lyon 1, UMR 5620 CNRS, F-69622 Villeurbanne, France*

[2]*Laboratoire de Spectroscopie Ionique et Moléculaire, Université de Lyon, Université Claude Bernard Lyon 1, UMR 5579 CNRS, F-69622 Villeurbanne, France*

[3]*Laboratoire Interdisciplinaire Carnot de Bourgogne, UMR 5209 CNRS–Université de Bourgogne, 9 avenue A. Savary, BP 47870, F-21078 DIJON Cedex, France*

[4]*Laboratoire de Physique de la Matière Condensée et Nanostructures, Université de Lyon, 43 Boulevard du 11 novembre 1918, Université Claude Bernard Lyon 1, F-69622 Villeurbanne, France*

(Received 12 December 2011; revised manuscript received 2 February 2012; published 18 May 2012)

Several populations of Cu spherical nanoparticles grown in a silicate glass at different temperatures with respect to the glass transition temperature were studied using high-resolution, low-frequency Raman scattering and optical absorption. The analysis of the spectra shows that the annealing of the doped glass at temperatures close to T_g leads to the formation of metallic copper nanoparticles with high crystallinity, whereas lower-temperature and higher-temperature annealings result in the formation of poorer nanoparticle assemblies in terms of size distribution and/or nanocrystallinity. It is also shown that in the case where the optical data do not unambiguously reveal the presence of metallic Cu nanoparticles, the Raman probe enables us to probe their presence as a result of the resonance process.

DOI: 10.1103/PhysRevB.85.205435 PACS number(s): 63.22.−m, 78.30.−j, 78.67.Bf

I. INTRODUCTION

Noble-metal nanoparticles (NPs) exhibit a large variety of optical properties that essentially arise from their surface-plasmon resonance (SPR). An original outcome of the SPR from metallic NPs is the ability to enhance Raman scattering through resonance conditions for the collective vibration modes whose wavelengths compare with the dimensions of the nano-objects. These vibrations depend on the morphology of the NPs (size, shape, composition) and also on the coupling with the surrounding of the NPs, as do the optical properties. The study of these vibrations therefore offers a complementary characterization to optical characterizations, providing an insight into elastic properties rather than electronic ones. In fact, the detection of NP low-frequency vibration modes has emerged as a very relevant probe whenever a direct characterization of NP assemblies through imaging techniques like transmission electron microscopy (TEM) is tedious to achieve. Such is the case when the NPs are buried in a matrix which becomes even worse as the density of NPs is significantly low. Previous studies[1,2] based on samples that allowed TEM characterization (i.e., with high NP densities) assessed the reliability of the low-frequency Raman scattering (LFRS) measurements for NP characterization in terms of size determination essentially. More interestingly, recent experimental investigations[3–8] have shown that probing the elastic properties of NPs through their low-energy vibration modes allows us to provide deeper characterization with respect to the NPs crystalline quality. In agreement with a recent complete theoretical analysis,[9] it was demonstrated that dealing with an assembly of NPs with good cubic lattice crystallinities, one could detect the lifting of degeneracy of the main Raman active mode induced by the elastic anisotropy of the crystalline nanostructures: the fundamental quadrupolar mode splits into two components having, respectively, E_g and T_{2g} symmetries. These pioneering studies have established the ability of LFRS to characterize NPs, including in the case of embedded NPs.[3,7,8]

This paper aims to exploit the ability of NP crystallinity characterization through low-frequency Raman scattering in the extreme case where metallic NPs are dispersed in a silicate glass at very low concentrations (typically lower than $\sim$100 NPs μm^{-3}), i.e., where a complete TEM characterization is virtually impossible. The metallic NPs are copper NPs, for which low-frequency Raman scattering studies are less documented[10] compared to gold or silver NPs. Nevertheless, red copper glasses are still an important part of colored glass manufacturing,[11] as alternatives to Cd-based red glasses or gold ruby glasses.[12] As a noble metal, copper is well suited for resonant low-frequency Raman scattering, while in terms of elastic anisotropy, its Zener ratio lies in the same range as that of gold or silver; therefore Cu NPs appear well suited to check the effect of nanocrystallinity on the low-frequency Raman spectra.

In this study, we report on the evolution of Cu NPs nucleated in glass through various thermal annealings by means of low-frequency Raman scattering, surface-plasmon characterization, and transmission electron microscopy. We show that, depending on the annealing temperature, with respect to the embedding glass transition temperature, significantly different Cu NP populations, essentially in terms of size and crystalline quality, are produced. As a result, we show that the low-frequency Raman probe allows detecting the presence of metallic nanoparticles even though the optical response is essentially dominated by the signature of copper oxide.

II. SAMPLES AND EXPERIMENTAL MEASUREMENTS

A. Samples

In order to assess the changes of the Raman spectra with the crystallinity of the NPs, different batches of samples

TABLE I. Preparation conditions of the five batches of investigated samples. The glass transition temperature of the sample is 560 °C.

Batch	Temperature (°C)	Annealing Heating rate (°C/min)	Time (h)
1	525	10	1–80
1A	525	25	2–8
2	700	10	0.5–8
3	580	25	0.5–90
4	525–700	25[a]	2

[a]The cooling rate for the samples of batch 4 was significantly lower than for the other batches.

corresponding to different growth conditions were investigated. Starting from a Cu-containing initially transparent silicate glass, annealing at temperatures below or above the glass transition temperature and over different times leads to differing Raman signatures and therefore different NP populations.

All samples reported in the study originate from a common colorless silicate glass prepared from a mix of main oxides with relative compositions (wt %) of $72SiO_2$-$15Na_2O$-9CaO-$2K_2O$-$1Al_2O_3$. Copper is initially incorporated as red cuprous oxide Cu_2O with 0.07 mol % concentration in the presence of minute quantities of urea as a reducing agent. The glass transition temperature T_g of the considered glass is 560 °C, as determined by differential scanning calorimetry.

Five batches of samples were investigated. Table I summarizes the preparation conditions of the five batches.

For all batches, the samples were annealed under atmospheric pressure, and the samples were allowed to cool down to room temperature inside the furnace after the heat was turned off. While batches 1, 1A, 2, and 3 are prepared with a fixed annealing temperature over different times, batch 4 deals with samples annealed at different temperatures over a fixed time of 2 h. For this latter batch, the cooling rate of the furnace was much lower than the one used for the preparation of the other batches, which, as explained in Sec. III D, leads to slightly different sizes from the 2-h annealed equivalent samples of the other batches.

B. Spectroscopic measurements

Since, in the case of noble-metal NPs, resonant Raman scattering infers from the coupling of the NP vibrations with the SPR,[13] it is important to characterize the optical densities of the samples. The optical absorption spectra were measured at room temperature over the 400–800-nm spectral range. All displayed spectra reflect the absorbance of the samples (copper NPs and glassy matrix). Due to the intense absorption of copper NPs, the thicknesses of the investigated samples were adjusted to between 0.5 and 1 mm.

The LFRS measurements were performed with a six-pass tandem Fabry-Pérot interferometer, working at mirror spacings ranging between 0.15 and 0.32 mm in order to cover spectral ranges of ±1000 and ±470 GHz, respectively, with differing resolving powers. In these conditions, the high optical contrast and resolving power of the instrument allow us to resolve inelastic signals off the quasielastic one from about 30 GHz, with a higher resolution than typical grating monochromators. All spectra were recorded with an incident wavelength $\lambda = 532$ nm, i.e., about 30 nm off the SPR maximum, with an incident power of 150 mW. All measurements were achieved in the backscattering geometry. In order to identify the origins of the different Raman bands, the spectra were recorded in either polarized (VV) or depolarized (VH) conditions using the vertical polarization of the laser light and placing a polaroid filter in a collimated path of the collected light.

In order to characterize the effect of embedding on the low-frequency modes of the NPs, the determination of the longitudinal and transverse sound velocities of the surrounding glass was needed. These were experimentally determined through Brillouin scattering using the same Fabry-Pérot setup with a typical mirror spacing of 3 mm. The measurements were also performed in the backscattering geometry so that the sound velocities V were derived from the relation $V = \nu_{\mathrm{Brill}}\lambda/(2n)$, where ν_{Brill} is the detected Brillouin shift, $\lambda = 532$ nm, and n is the refractive index. For all samples, n was measured independently from m-line spectroscopy and was found to equal 1.523.

C. Transmission electron microscopy

In order to tentatively check the morphology of the NPs, TEM samples were prepared using the diamond-tip scratching method. TEM observations were carried out using a Topcon EM-002B instrument at 120 kV. As already emphasized in the Introduction, due to the very low concentration of NPs in the glass volume and to the low TEM contrast of metal NPs embedded in glass, good-quality TEM pictures were difficult to obtain. The TEM pictures shown therein only correspond to reliable data, i.e., obtained with reasonable reproducibility. They are to be considered as qualitative supporting information to the Raman analysis, which remains the main tool of interpretation.

III. RESULTS AND ANALYSIS

A. Annealing below T_g

Figure 1 displays the optical absorption and Raman results obtained on the samples annealed during different times *below* the glass transition temperature (batch 1). Figure 1(a) proves the presence of metallic copper NPs through the presence of the corresponding SPR at 560 nm, in accordance with the red color of the samples.

In order to estimate the volume fraction q of the Cu involved in the formation of the NPs in the glass, and hence the NP density, the experimental absorbance spectra were compared with curves theoretically calculated by the Maxwell-Garnett theory (effective medium theory)[14] based on the complex dielectric constant of the considered NP metal. For the sole purpose of the estimation of q, the calculated curves need not be fitted to the data by adjusting parameters like the refractive index of the surrounding medium in the close vicinity to the NPs. The only input parameters that were kept fixed in the calculations were the experimentally determined macroscopic refractive index of the matrix n and the unique size of the NPs, which is that derived from the Raman measurements. Note

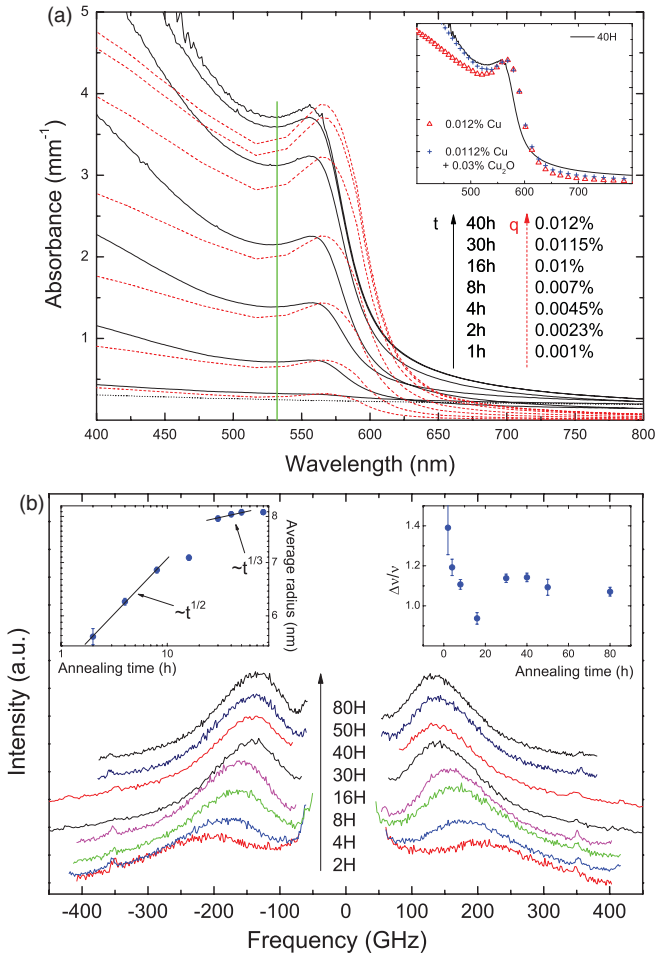

FIG. 1. (Color online) Batch 1: samples annealed below T_g. (a) Absorption spectra showing the SPR at 560 nm. Solid black curves are experimental spectra, dashed red curves are spectra calculated using Maxwell-Garnett theory, and the vertical line is the wavelength used to perform the resonant Raman measurements. The dotted black line is that of the transparent glass before annealing. The inset shows the experimental (solid line) and calculated absorbance curves using Cu NPs only (triangles) or an admixture of Cu and Cu_2O NPs (crosses) with respective volume fractions of 0.0112% and 0.03%. (b) LFRS VV spectra; the spectra are shifted along the vertical axis for clarity. The left inset shows the evolution of the NP average radius with annealing time (log-log plot). The right inset shows the dependence of the ratio $\Delta\nu/\nu$ on the annealing time.

that in the investigated size regime (approximately $10 < D < 20$ nm), where multipolar ($D > 50$ nm) and quantum effects ($D < 3$ nm) do not come into play, the size (and hence a size distribution) of the absorbing Cu NPs has virtually no effect on the absorbance profiles.[15]

The calculated curves appear to be in good qualitative agreement with the experimental ones, considering the use of nonadjustable parameters. The disagreement of the SPR positions between experimental and calculated curves may be the result of different effects: NP size and shape distributions and, most importantly, the interface between the NPs and the embedding glass, which may lead to a local effective refractive index that differs from the one measured macroscopically. Furthermore, the different behaviors of the experimental and calculated curves below 550 nm can be explained by the partial oxidation of copper. Indeed, it is known[12] that during heating at temperatures lower than 1100 °C in an oxidizing atmosphere, Cu reacts with oxygen and forms copper (II) oxide and copper (I) oxide. Cupric oxide is not very stable, and under the influence of temperature it is reduced to copper (I) oxide, which is more stable. Moreover, the coformation of Cu_2O NPs and Cu NPs in silica glasses is well known.[16,17] We indeed observe that calculating the total absorbance of an admixture of Cu and Cu_2O NPs more adequately describes the experimental data, as shown in Fig. 1(a) for the 40-h sample.

Whatever the annealing time, the Raman spectra [Fig. 1(b)] show a single broad component that shifts toward lower frequencies upon increasing the annealing time. The band profile is observed to be independent of the polarization conditions so that, as is well known from the low-frequency Raman scattering of NPs, this band can be safely assigned to the fundamental spheroidal quadrupolar mode of the NPs. Assuming the NPs as nanospheres the frequency ν of the spheroidal modes is given by

$$\nu_{n,\ell} = S_{n,\ell}\frac{V_T}{D}, \tag{1}$$

where the indices ℓ and n respectively refer to the angular momentum and harmonic order of the considered spheroidal mode, V_T is the transverse speed of sound, and $D = 2R$ is the diameter of the vibrating sphere. In the case of freely vibrating nanospheres, the frequency of the fundamental ($n = 1$) quadrupolar ($\ell = 2$) mode is obtained using $S_{1,2} = 0.84$. This factor was shown to evolve for spheres embedded in a matrix.[18,19] It can be computed using the complex frequency method (CFM) inputting the elastic and density parameters of the matrix. For the considered glass, $\rho = 2.48$ g cm^{-3} and the sound velocities measured through Brillouin scattering are $V_L = 5730$ m/s and $V_T = 3480$ m/s. Using the CFM approach, the value of the $S_{1,2}$ factor is shifted to 0.95 for metallic Cu NPs. The left inset of Fig. 1(b) shows the evolution of the average radius as a function of annealing time, as deduced from Eq. (1). Basically, two stages are identified: in the first stage (2–16 h) the average NP radius increases quite rapidly (0.2 nm/h) with respect to the second stage (30–80 h), where the radius only very slightly increases (0.003 nm/h). This two-stage evolution is also found in the dependence of the relative spectral width $\Delta\nu/\nu$ ($\Delta\nu$ is the full width at half maximum derived from a Lorentzian fit of the data) of the Raman band with annealing time [right inset of Fig. 1(b)]. The value of $\Delta\nu/\nu$ is found to strongly decrease for annealing times ranging between 2 and 16 h, while it remains almost constant for longer annealing times.

The two-step evolution observed in the LFRS complies with the scenario generally involved for the growth of NPs during isothermal annealing.[20] In a first regime, NPs grow according to a precipitation process of a supersaturated solution. Once the size of the NPs is fairly large, as the degree of supersaturation becomes very small, large particles further grow at the expense of smaller ones that dissolve. This latter stage is called *coarsening*, or Ostwald ripening, and is basically governed by a Gibbs-Thomson effect according to which smaller NPs (or clusters) have a higher solubility.

The main growth stage is a pure diffusional process. In this regime the evolution of the average radius obeys a $(Dt)^{1/2}$ law,[20] where D is the diffusion coefficient of the Cu atoms and t is the diffusion time. The inset of Fig. 1(b) shows that this trend is indeed qualitatively observed. Besides the rapid growth of the NPs in this first regime, the significant reduction of the Raman band width indicates that, at the same time, the heterogeneity of the NP assembly becomes significantly lower. This may be due to a narrowing of the size dispersion [$\Delta\nu/\nu = \Delta D/D$ along Eq. (1)] or to an improvement of NPs inner crystallinity with annealing.[1]

In the following stage, both the average size [Fig. 1(b), left inset] and the size distribution [Fig. 1(b), right inset] of the formed NPs hardly evolve. In this "ripening" process, the Cu transfer occurs from the smaller clusters to the largest ones. The apparent nonevolution of the Raman band profile, which can reasonably be assumed as a probe of size dispersion, indicates that the dissolving smallest aggregates initially had a negligible contribution to the observed Raman signal. Such is reasonable if one considers that due to the resonant Raman process, the coupling with the surface-plasmon excitation favors the response of the larger NPs, as the polarizability of a NP is proportional to its volume.[21,22] In the coarsening regime, the average radius is expected to scale with a $(Dt)^{1/3}$ law.[20] Qualitatively, this trend is observed in our data [left inset of Fig. 1(b)].

On the basis of these observations, it is interesting to check if the increase of the NP average size in the coarsening regime is consistent with the Cu volume fractions determined from the fits of the absorption spectra. According to its definition, the NP Cu volume fraction for a given annealing time t_a can be approximated by

$$q_{t_a} \sim \frac{N_{t_a}\langle V_{t_a}^{1NP}\rangle}{V_{\text{glass}}}, \tag{2}$$

where N_{t_a} is the number of NPs with average volume $\langle V_{t_a}^{1NP}\rangle$ embedded in the glass volume V_{glass}. Considering that in the ripening process the number of dominating NPs is almost unchanged, one obtains the q ratio for two annealing times t_1 and t_2:

$$\frac{q_{t_1}}{q_{t_2}} \approx \frac{R_{t_1}^3}{R_{t_2}^3}, \tag{3}$$

where R_{t_1} and R_{t_2} are the Raman-determined NP radii [Eq. (1)] for annealing times of t_1 and t_2, respectively. Using the values found for 30 and 40 h of annealing, the ratio $\frac{q_{40h}}{q_{30h}} \approx 1.043$, derived from the absorbance data, is found to compare reasonably well with the ratio $\frac{R_{40}^3}{R_{30}^3} \approx 1.038$ derived from the positions of the Raman bands.

From Eq. (2), it is instructing to derive the NP density N_{t_a}/V_{glass} on the basis of the average size determined by the Raman quadrupolar band [Fig. 1(b), left inset]. Assuming the NPs are spheres, the number density of Cu NPs is found to evolve from about 30 to 55 NPs μm^{-3} between 2 and 40 h of annealing. As emphasized earlier, these values are extremely low compared to typical NP studies.[23]

In order to investigate the influence of the heating rate on the grown NPs, an extra batch (1A) of samples that were annealed at 525 °C but with a heating rate greater than that of batch 1 (25 vs 10 °C/min) was prepared. Figure 2 compares the LFRS spectra of series 1 and 1A for small annealing times. Figure 2 shows well that the heating rate does not appreciably influence the Raman profiles. The only difference which may be remarked is a slight blueshift of the bands with batch 1A at small annealing times. This is consistent with the fact that a higher heating rate leads to the formation of more nucleation centers with smaller sizes in the glass.

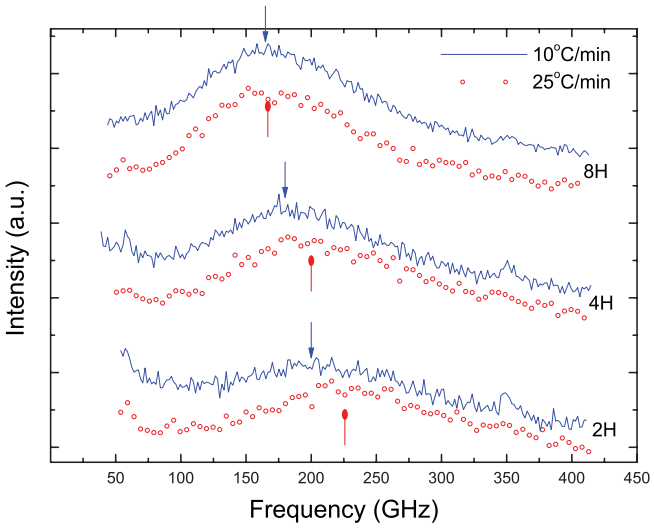

FIG. 2. (Color online) LFRS spectra of batches 1 (solid lines) and 1A (circles): samples were annealed below T_g at two different heating rates.

Overall, annealing of the Cu-doped glass at temperatures lower than its glass transition temperature results in the formation of metallic-copper NPs characterized by a fairly large size distribution. Because of this, it is impossible to probe the fine details of the NP structure or to detect the spherical mode ($n = 1, \ell = 0$). As shown next, this situation significantly differs from annealing the samples well above T_g.

B. Annealing well above T_g

Figure 3 shows the results obtained from the samples annealed at a temperature well above T_g (batch 2). Unlike the results of batch 1, the absorption curves do not evidence any SPR [Fig. 3(a)]. Visually, these samples are brown, while the batch 1 samples are red. The same result was obtained in Ref. 11 for glasses doped with Cu_2O.

Obviously, the smooth absorption curves of Fig. 3(a) reflect the presence of copper oxide in the glass. Yet associating the smooth absorbance curves with a defined type of NP (oxide NP or metal/oxide core/shell structure) is difficult. Indeed, core-shell NPs made of a metallic copper core and an oxide outer shell are expected to feature a defined SPR peak,[24] which is not observed in the spectra of Fig. 3(a). On the other hand, assuming a mixture of Cu NPs and Cu_2O or CuO NPs does not satisfactorily describe the experimental data either [symbols in Fig. 3(a)]. Finally, it could be that a weak SPR signal from Cu NPs is masked by a dominating contribution from copper oxide(s). Therefore, at this stage, we will assume that the sample may contain three types of NPs: Cu, CuO, and Cu_2O.

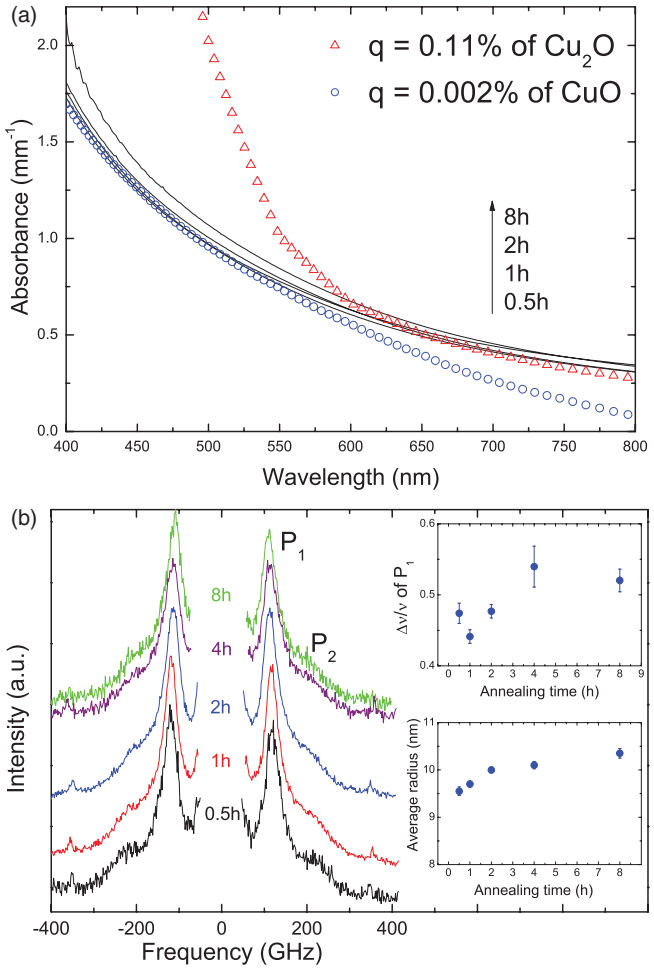

FIG. 3. (Color online) Batch 2: samples annealed well above T_g. (a) Absorption spectra: experimental curves (solid lines), Maxwell-Garnett calculated curves for CuO (circles), and Cu_2O (triangles). (b) LFRS VV spectra; the spectra are normalized on the maximum and shifted along the vertical axis for clarity. The bottom inset shows the evolution of the NP average radius with annealing time. The top inset shows the dependence of the ratio $\Delta\nu/\nu$ of the P_1 peak on the annealing time.

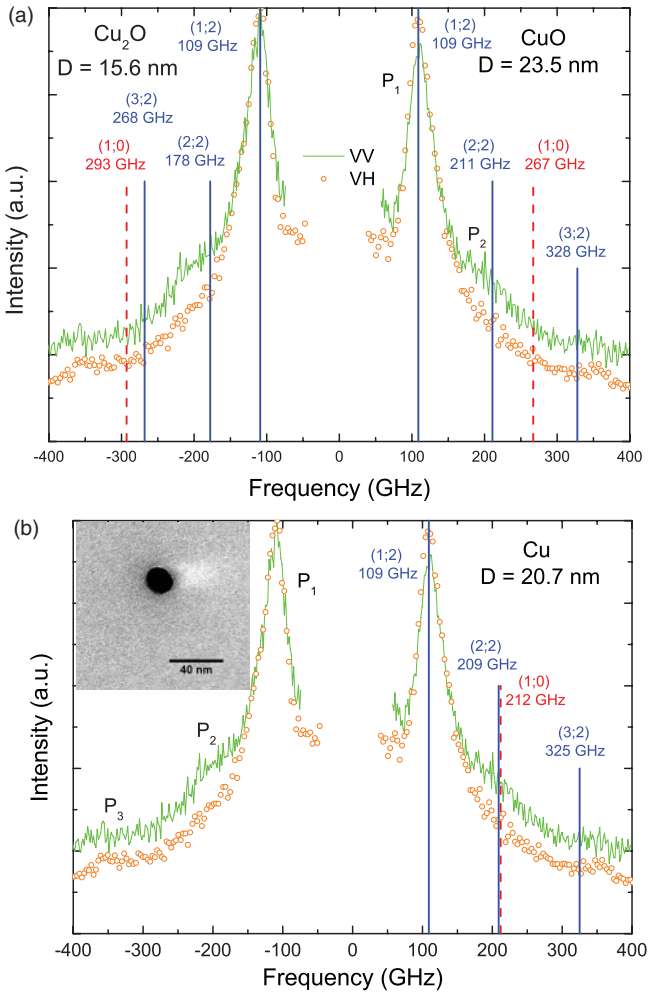

FIG. 4. (Color online) Polarized (solid lines) and depolarized (symbols) LFRS spectra from the sample annealed at 700 °C for 8 h (batch 2). The spectra are normalized on the maximum intensity. The bars are the theoretical CFM predictions of the spherical ($\ell = 0$) and of the quadrupolar ($\ell = 2$) modes, together with their overtones n [(n,ℓ) notation]. The heights of the bars are irrelevant to intensities. (a) Cu_2O and CuO NPs assumptions are respectively indicated on the negative and positive frequency sides of the Stokes/anti-Stokes spectrum. (b) Cu NPs assumption. The inset shows the TEM image of the sample.

The LFRS spectra (VV configuration) of the batch 2 samples are represented in Fig. 3(b). Each spectrum contains two bands, marked in Fig. 3 by P_1 (around 100–120 GHz) and P_2 (around 200–230 GHz). It is obvious that the main peak P_1 is significantly narrower than that of the samples from batch 1, as shown by its relative frequency width [Fig 3(b), right inset] with respect to that of the main peak of batch 1 samples [Fig 1(b), top inset]. Compared to Fig. 1(b), the redshift of the observed bands with increasing annealing time is small [Fig. 3(b), bottom inset].

The different components of the spectra (P_1, P_2) are identified by comparing the VV and VH spectra. Figure 4 shows this comparison with the largest annealing time sample. As can be seen, P_1 is depolarized, while P_2 is polarized. Therefore P_1 can be identified as the fundamental quadrupolar mode ($n = 1; \ell = 2$), while P_2 is ascribed to the fundamental spherical mode. The observation of the spherical mode confirms the narrow size distribution of the formed NPs and their good crystallinity, as previously observed with Ag-embedded NPs.[25]

As already stated, the optical absorption spectra [Fig. 3(a)] do not unambiguously unveil the presence of Cu NPs due to the nonvisibility of a SPR peak. The smooth absorption curves are suspected to reflect the presence of Cu_2O and/or CuO. In the following, a comparison of low-frequency mode calculations performed with either pure Cu NPs or pure Cu_2O and pure CuO NPs is presented. It shows that the detected vibrations comply essentially with those of pure Cu NPs.

Figure 4 indicates the frequency positions calculated using the CFM, with the appropriate matrix parameters. The size of the NPs was set such that the position of the main P_1 peak coincides with that calculated for the ($n = 1; \ell = 2$) mode. The comparisons with the Cu_2O and CuO assumptions are respectively performed on the negative and positive frequencies

TABLE II. Parameters used for CFM calculations of vibrational modes of Cu, CuO, and Cu_2O NPs.

Substance	V_L (m/s)	V_T (m/s)	ρ (g/cm^3)
Cu	4799	2381	9.02
CuO (Ref. 26)	6600	2700	6.32
Cu_2O (Ref. 27)	4499	1363	6.07

of the Stokes/anti-Stokes spectrum shown in Fig. 4(a), and the CFM calculations for Cu NPs are reported in Fig. 4(b). The averaged elastic parameters used for these calculations are displayed in Table II.

As can be seen from Fig. 4, a better agreement is obtained with the Cu NPs assumption. Indeed, once the size of the NP is fixed, through the position of the quadrupolar mode, the associated frequency of the spherical mode better matches the experimental one assuming Cu NPs. It also enables the identification of a very weak band near 350 GHz [P_3 band in Fig. 4(b)] as the third harmonic of the quadrupolar mode.

From the above analysis, we can conclude that in spite of the presence of copper oxides in the sample, which are strongly suggested by absorption measurements, the analysis of the Raman signal suggests that the detected vibrational modes arise from *metallic* Cu NPs. It is very possible that the volume fraction of Cu NPs produced through annealing in a highly oxidizing atmosphere is very small in comparison with copper oxide, so that the associated SPR signal is masked in the absorbance spectra. On the other hand, due to the resonant Raman conditions, the selective response of the Cu NPs is observed.

Once the data of Fig. 3(b) are interpreted with the assumption of Cu NPs, we derive that the size of the NPs increases from $D \approx 19.1$ nm to $D \approx 20.7$ nm between 0.5 and 8 h of annealing at 700 °C [bottom inset of Fig. 3(b)]. Besides the fact that these sizes are 30% to 60% larger than those produced through annealing below T_g, the overall Raman profile is very different, as shown by the $\Delta\nu/\nu$ values [top inset of Fig. 3(b)]. The narrow profile of the quadrupolar mode ($\Delta\nu/\nu \sim 0.5$) definitely appears as a prerequisite for the observation of the spherical mode.

In order to crosscheck the size of the Cu NPs, we performed tentative TEM measurements, considering that the obtention of the images is nontrivial due to both the highly diluted assemblies and the embedding silicate glass. The inset of Fig. 4(b) shows a TEM micrograph obtained on the sample of batch 4 annealed for 2 h at the same temperature as samples of batch 2, i.e., 700 °C (as in Fig. 2, for short annealing times, the different heating rates of the two series have no significant influence on the observed Raman spectra). The size deduced from the TEM observation is of the order of 20 nm, i.e., in very good agreement with that deduced from the Raman spectrum [Fig. 3(b)].

Although the sizes of the Cu NPs formed at 700 °C compare with those previously detected in similar AgAu (Ref. 7) or Au (Ref. 3) NPs embedded in glass, no effect of elastic anisotropy could be detected: the quadrupolar mode consists of an unsplit single narrow line. This suggests that the Cu NPs are not single nanocrystals (NCs) but rather polycrystalline or at least multiply twinned particles (MTPs).[5] One essential difference between the Au or AuAg samples reported before[3,7] and the present Cu sample batch is that the former samples were produced through annealing *close to* T_g. In order to check whether the detection of the elastic anisotropy effect relates to an annealing closer to T_g we now focus on the results obtained from samples annealed slightly above T_g (batch 3).

C. Annealing around T_g

Absorption spectra of the samples annealed at a temperature slightly above T_g (batch 3) are shown in Fig. 5(a). As observed on the spectra of the samples annealed below T_g, these samples also demonstrate a visible SPR peak at the position around 557 nm, thereby proving the existence of Cu NPs. The absorption profiles of the samples annealed around T_g roughly behave like those of the samples annealed at a temperature lower than T_g [Fig. 1(a)], except that the SPR appears slightly more damped and less intense at the latest stages of annealing in the case of batch 3. This observation can be interpreted as

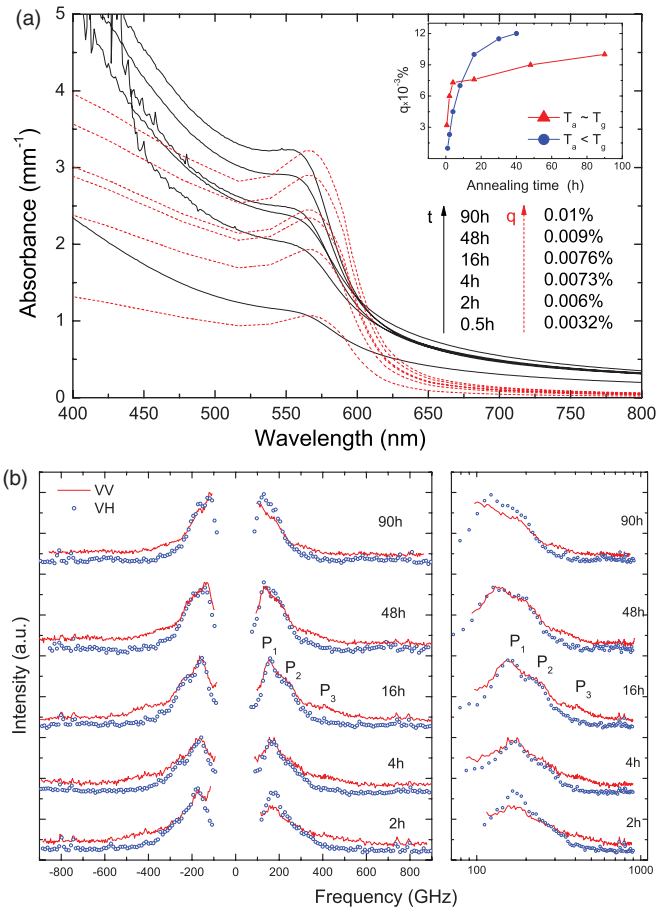

FIG. 5. (Color online) Batch 3: samples annealed slightly above T_g. (a) Absorption spectra showing the SPR at 560 nm. The symbols are as in Fig 1(a). The inset shows the evolution of Cu NP volume fraction q with annealing time for batch 1 (circles) and batch 3 (triangles). (b) Left: Polarized/depolarized LFRS spectra on linear scale. Right: Log-linear representation of the Stokes side better evidencing the P_1, P_2 doublets.

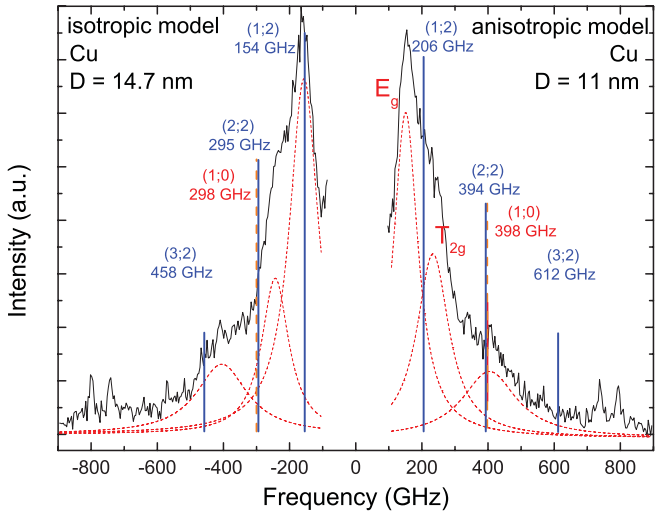

FIG. 6. (Color online) Polarized LFRS spectra from the sample annealed slightly above T_g (580 °C) for 16 h (batch 3) compared with CFM predictions [same notation as in Fig. 4(b)].

poorer distributions of NP sizes or of local NP environments and/or as an additional presence of copper oxide whose smooth absorbance curves [Fig. 3(a)] damp the SPR.

Comparing the values of copper volume fractions q for batches 1 and 3, we can see that the increase of q proceeds differently [inset of Fig. 5(a)]. During the first hours of annealing the amount of copper involved in Cu NPs is higher for the samples annealed near T_g. This is most probably due to the more efficient diffusion of Cu atoms in the disordered, less rigid glass structure compared to samples annealed below T_g. At 20–40-h annealing time, the sample annealed below T_g shows a higher Cu NP volume fraction. This is a sign that in the sample annealed above T_g part of the copper atoms is not involved in the formation of Cu NPs. Indeed, a competitive process of metallic Cu NP formation is Cu oxidation (leading to either Cu_2O NPs or metallic core/oxide shell NPs), which is expected to be enhanced at the higher annealing temperature.

The LFRS spectra of this series are displayed in Fig. 5(b). Each VV spectrum shows three components (P_1, P_2, P_3), among which one (P_3) appears polarized from the VV/VH comparison. Comparing these spectra with those recorded for samples annealed below T_g and well above T_g, the following remarks can be made.

(i) The main contribution to the spectrum ($\nu < 350$ GHz) definitely shows a double-component structure, similar to that already observed on comparable systems made of highly crystalline NPs.[3,5,7,8] It is therefore natural to interpret it as a signature of elastic anisotropy in the present case of Cu NPs.

(ii) The barycenter of this double-component feature typically lies at frequencies larger than those observed for the previously investigated systems. This means that the corresponding NPs size is smaller.

Considering the absorption results obtained for the present series of samples and from the previous analysis performed for samples annealed well above T_g, we discard from the outset an interpretation of the Raman data based on copper oxide NPs. As indicated by Fig. 6 (left side), interpreting the lowest-frequency peak P_1 as a unique ($n = 1; \ell = 2$) mode from a NP of diameter 9.5 nm, within the CFM, fails to reproduce the frequency positions of the P_2 and P_3 bands. One therefore turns to the elastic anisotropy effect. Fitting the three observed components with Lorentzian profiles allows us to evaluate the frequency ratio of the E_g-T_{2g} doublet. The average value of this ratio obtained from fits of the five curves displayed in Fig. 5(b) is $\nu_{T_{2g}}/\nu_{E_g} \approx 1.53$, which is in very good agreement with the recently published predicted value of 1.51,[8] which takes into account the effect of the matrix on the E_g-T_{2g} splitting. In order to predict the positions of the spherical mode and of the quadrupolar mode harmonics, the E_g-T_{2g} doublet is modeled as a single band with a barycenter that takes into account the degeneracy of the E_g and T_{2g} components:

$$\left\langle \nu_{E_g - T_{2g}} \right\rangle \approx \frac{2\nu_{E_g} + 3\nu_{T_{2g}}}{5}. \quad (4)$$

The results are shown as vertical bars on the positive-frequency side of Fig. 6. Obviously, the agreement with experimental data is very satisfactory and is summarized as follows.

(i) The P_1 and P_2 peaks respectively arise from the E_g and T_{2g} components of the split ($n = 1; \ell = 2$) quadrupolar mode. The NP diameter is around 11 nm.

(ii) The P_3 peak, observed in VV configuration only, arises from the fundamental ($n = 1; \ell = 0$) spherical mode. Note that the P_3 peak position coincides with that of the ($n = 2; \ell = 2$) mode, which is not observed in the depolarized spectra.

The comparison of these results with those obtained from previous batches reveals that the formed NPs significantly depend on the annealing temperature. Annealing the transparent glass well above its glass transition temperature (batch 2) leads to the formation of large Cu NPs in somewhat reduced proportion compared to the presence of copper oxide, which dominates the optical response. However, the size is not the only parameter to change. While the elastic anisotropy effect appears clearly when the annealing is performed close to T_g, it is no longer observed when the annealing is performed far above T_g. Before proceeding to a structural interpretation of these observations, we present the results obtained on samples annealed for a fixed time of 2 h at temperatures ranging between lower than T_g and well above T_g (batch 4).

D. Annealing for a fixed time

Figure 7(a) presents the absorption spectra of the samples of batch 4. The obvious SPR peak is observed only for the samples annealed at temperatures lower than or close to T_g, while it becomes less and less visible with an increase of the annealing temperature. This result confirms that the higher the annealing temperature is, the more Cu atoms oxidize. When temperature lies above 605 °C the absorption signal does not show a defined SPR maximum any longer, as observed previously (batch 2). The larger absorbance of the sample annealed at 630 °C compared to that of the one annealed at 700 °C is the result of a more active formation of copper oxide particles to the detriment of Cu atoms and Cu NPs.

Figure 7(b) shows the LFRS of samples annealed for 2 h at different temperatures. Qualitatively, these measurements are fully consistent with those obtained from the previous series at 2 h of annealing. As observed with the three previous batches of samples, the NPs annealed below T_g have a very poor Raman

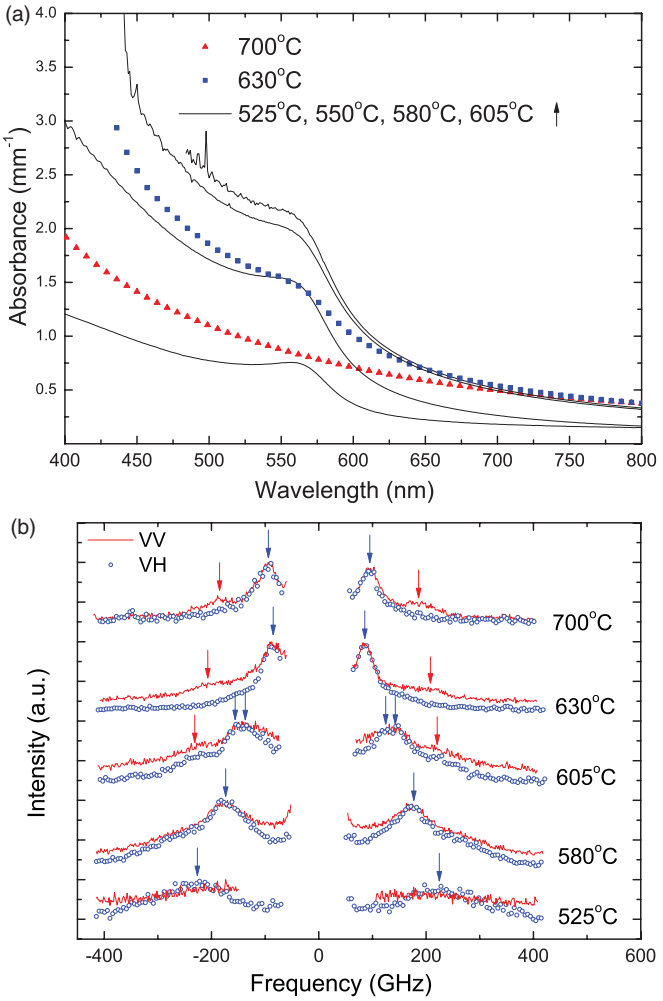

FIG. 7. (Color online) Batch 4: samples annealed for a fixed time of 2 h. (a) Absorption spectra: the experimental spectra of the sample annealed at low temperatures (solid lines), at 630 °C (squares), and at 700 °C (triangles). (b) Polarized/depolarized LFRS spectra; the spectra are normalized on the maximum and shifted along the vertical axis for clarity.

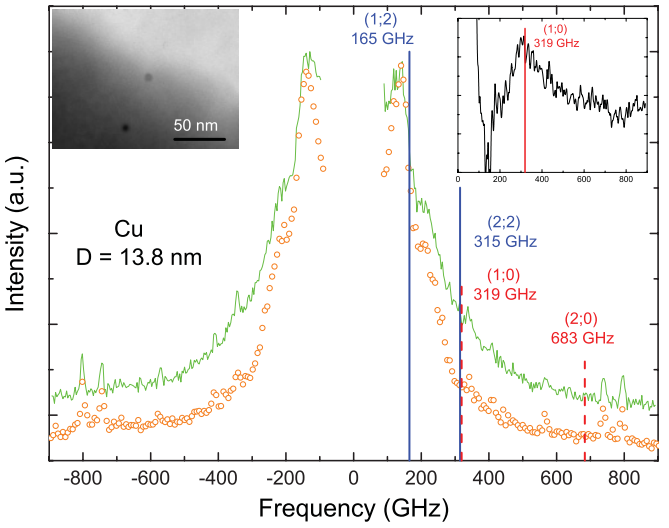

FIG. 8. (Color online) LFRS VV (solid line) and VH (symbols) spectra from the NPs annealed at 605 °C for 2 h [same spectrum as in Fig. 7(b) with another free spectral range] and the theoretical CFM prediction of the frequency positions of the vibrational modes and their harmonics for Cu NPs with an average size of 13.8 nm with the assumption that the NPs are single crystals. The left inset shows a TEM image of the sample. The right inset shows the difference spectrum $I_{VV} - kI_{VH}$, where k is a normalizing coefficient.

response with a very broad single band in the spectrum. In the end portion of the T_g zone, i.e., 580–605 °C, one can observe the splitting of the quadrupolar mode with a T_{2g}/E_g ratio of 1.53–1.54, i.e., close to that already observed. Passing to higher temperatures (630–700 °C), the Raman spectrum shows a narrow quadrupolar mode with no signature of elastic anisotropy, and the contribution of the spherical mode becomes clearly visible. In fact this contribution can be detected already from the sample annealed at 605 °C.

A close look at the comparison VV/VH spectra for this sample (Fig. 8) unveils the presence of a polarized signal which is better evidenced in the difference spectrum $I_{VV} - kI_{VH}$ (right inset of Fig. 8). The position of this signal is very close to that predicted by CFM (red bar) for the spherical mode ($n = 1; \ell = 0$) of the Cu NPs with size $D = 13.8$ nm, which is in good agreement with TEM measurements of the same sample (left inset of Fig. 8). Definitely, it appears from Fig. 7(b) that the visibility of the spherical mode strongly depends on the width of the quadrupolar line (or its corresponding E_g-T_{2g} doublet): the broader the quadrupolar contribution is, the weaker the spherical mode signal is. One observes that once a minimum linewidth is reached, or as soon as the annealing is performed above T_g, the lines become sufficiently narrow for the spherical mode contribution to materialize. This trend could not be observed from batch 2 [Fig. 3(b)] since from the very first sample (0.5 h of annealing) a minimum large linewidth appeared to have already been reached.

Quantitatively, the NP sizes obtained for the samples of batch 4 annealed near and far above T_g are about 30% larger than those derived from batches 2 and 3 for the same annealing time of 2 h. As mentioned, this is attributed to the slower cooling rate of the furnace used to prepare samples of batch 4. For the lowest-temperature annealing (525 °C), the slower cooling rate has no influence.

The results obtained on the fourth batch of samples, as we noted above, have allowed us to follow the evolution of the LFRS spectra from low to high temperatures, reproducing the spectra of the first three series of the sample. From there, we are able to draw a general scheme for the formation of embedded Cu NPs through annealing.

IV. CONCLUSION

Figure 9 summarizes the sizes derived for the four batches of samples annealed for long times and gives a basic schematic representation of the corresponding Raman Stokes profiles. Starting from a colorless, Cu-doped glass, annealing at temperatures lower that T_g (batch 1), the LFRS spectra consist of a single broad band attributed to the quadrupolar mode of Cu NPs. The width of the quadrupolar mode reflects the large size

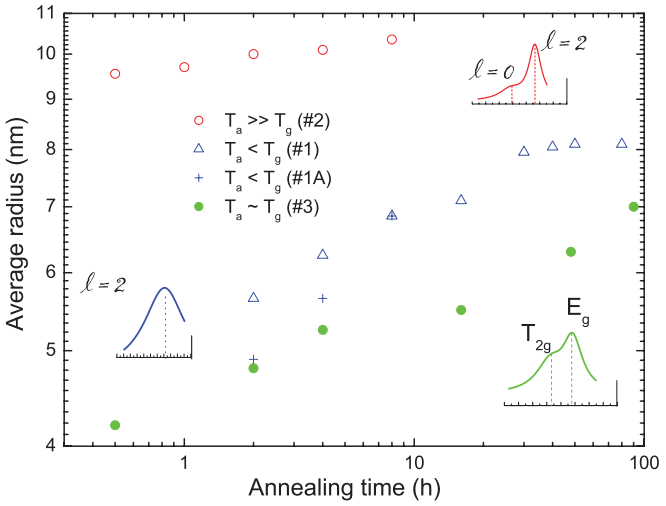

FIG. 9. (Color online) Evolution of the average radius as a function of annealing time assuming Cu NPs for the four series of the samples: batch 1 (triangles), batch 1A (crosses), batch 2 (open circles), and batch 3 (solid circles).

distribution of the formed particles. Obviously, at temperatures lower than T_g, the still solid behavior of the glass network hinders the diffusion of Cu atoms so that the formed NPs are likely to be poorly crystallized and hardly spherical, with a large size distribution. While this situation yields a poor Raman signal, it is worth noting that the associated optical response is rather well defined, with a clear SPR. Furthermore, prolonged annealing below T_g does not substantially improve the quality of the Raman signal, while a maximum average diameter of about 16 nm is reached. A larger heating rate (series 1A) does not appreciably change the Raman profile, and the only parameter it can influence is the size of the formed NPs. As mentioned, with an increase of the heating rate the NPs form in a larger amount but with smaller sizes. However, a long annealing time (see the 8-h point for batches 1 and 1A) leads to the vanishing of the heating rate's influence; i.e., the formed NPs possess the same diameter for different heating rates. This is caused by two probable reasons: the dissolving of the small spheres during ripening and the selection of the largest particles by Raman scattering. In order to significantly modify the Raman profile, one needs to increase the annealing temperature.

Annealing the glass slightly above its glass transition temperature (batch 3) leads to a more structured Raman response. The single broad maximum observed at lower annealing temperature transforms into a double-component structure. The two components identify with the E_g and T_{2g} modes that arise from the splitting of the quadrupolar mode when the NPs are NCs, i.e., featuring elastic anisotropy. At this temperature of annealing, the viscosity of the glass is such that the diffusion of Cu atoms is facilitated and they have sufficient energy to organize into crystal structures. The sizes obtained from the average position of the E_g-T_{2g} doublet, i.e., using an isotropic model of embedded nanospheres, are somewhat smaller than those obtained through annealing below T_g.

Annealing at temperatures well above T_g (batch 2) produces essentially narrow Raman lines. The E_g-T_{2g} doublet structure of the quadrupolar mode is no longer observed, and the spherical mode contribution is clearly visible in the polarized spectra; higher-order harmonics of the quadrupolar mode may also be detected. In a sense, the LFRS profiles are closer to those expected from elastically isotropic nanospheres, with a quite narrow size distribution. In comparison with lower-temperature annealings, the sizes obtained are larger. On the other hand, the nonobservation of the E_g-T_{2g} doublet testifies that NPs cannot be identified as single NCs. Therefore, these NPs are most likely polycrystals or MTPs of relatively large size, as opposed to the small NCs produced through annealing slightly above T_g. One may further suggest that the shapes of the polycrystalline NPs formed at high temperature are more spherical, in contrast to faceted ones. It is worth noting that in the case of high-temperature annealing, the optical absorption data do not reflect the presence of metallic Cu NPs, with the absence a defined SPR. Yet the quantitative Raman analysis based on the elastic signatures of metallic Cu, as compared to those of copper oxides, allows us to assess their presence.

The reported works have allowed us to draw a general picture of how thermal treatment used to generate color in Cu-doped glasses may produce different types of NPs in terms of size, size distribution, and nanoparticle crystallinity. The low-frequency Raman probe appears to be a convenient technique for this kind of system, where NPs are highly diluted and buried in an embedding medium that is hard to process with respect to TEM characterization. Improvements on its quantitative use, in particular with regard to biased size probing due to resonance conditions, appear to be necessary in order to substantiate low-frequency Raman characterization.

ACKNOWLEDGMENTS

The authors acknowledge S. Albert from St Just glass manufacture for kindly providing the initial doped glass and S. Belin for the DSC measurements.

[1]E. Duval, H. Portalès, L. Saviot, M. Fujii, K. Sumitomo, and S. Hayashi, Phys. Rev. B **63**, 075405 (2001).
[2]A. Courty, I. Lisiecki, and M. P. Pileni, J. Chem. Phys. **116**, 8074 (2002).
[3]B. Stephanidis, S. Adichtchev, S. Etienne, S. Migot, E. Duval, and A. Mermet, Phys. Rev. B **76**, 121404 (2007).
[4]Y. Tang and M. Ouyang, Nat. Mater. **6**, 754 (2007).
[5]H. Portalès, N. Goubet, L. Saviot, S. Adichtchev, D. B. Murray, A. Mermet, E. Duval, and M.-P. Pileni, Proc. Natl. Acad Sci. USA **105**, 14784 (2008).
[6]H. Portales, N. Goubet, L. Saviot, P. Yang, S. Sirotkin, E. Duval, A. Mermet, and M.-P. Pileni, ACS Nano **4**, 3489 (2010).

[7]S. Adichtchev, S. Sirotkin, G. Bachelier, L. Saviot, S. Etienne, B. Stephanidis, E. Duval, and A. Mermet, Phys. Rev. B **79**, 201402 (2009).
[8]L. Saviot, D. B. Murray, E. Duval, A. Mermet, S. Sirotkin, and M. C. Marco de Lucas, Phys. Rev. B **82**, 115450 (2010).
[9]L. Saviot and D. B. Murray, Phys. Rev. B **79**, 214101 (2009).
[10]K. E. Lipinska-Kalita, D. M. Krol, R. J. Hemley, G. Mariotto, P. E. Kalita, and Y. Ohki, J. Appl. Phys. **98**, 054301 (2005).
[11]P. Colomban and H. D. Schreiber, J. Raman Spectrosc. **36**, 884 (2005).
[12]T. Bring, Ph.D. thesis, Växjö University, 2006.
[13]G. Bachelier and A. Mlayah, Phys. Rev. B **69**, 205408 (2004).
[14]J. C. M. Garnett, Philos. Trans. R. Soc. London, Series A **205**, 237 (1906).
[15]E. Cottancin, M. Broyer, J. Lermé, and M. Pellarin, *Handbook of Nanophysics-Nanoelectronics and Nanophotonics* (CRC Press, Boca Raton, FL, 2011) Chap. 24, p. 24.
[16]N. Murase and T. Yazawa, J. Am. Ceram. Soc. **84**, 2269 (2001).
[17]O. A. Yeshchenko, I. M. Dmitruk, A. M. Dmytruk, and A. A. Alexeenko, Mater. Sci. Eng. B **137**, 247 (2007).
[18]D. B. Murray and L. Saviot, Phys. Rev. B **69**, 094305 (2004).
[19]L. Saviot, D. B. Murray, and M. C. Marco de Lucas, Phys. Rev. B **69**, 113402 (2004).
[20]G. De Marchi, G. Mattei, P. Mazzoldi, C. Sada, and A. Miotello, J. Appl. Phys. **92**, 4249 (2002).
[21]B. N. J. Persson and A. Liebsch, Phys. Rev. B **28**, 4247 (1983).
[22]E. Duval, A. Mermet, A. Courty, P. A. Albouy, and M. P. Pileni, Phys. Rev. B **72**, 085439 (2005).
[23]M. Cazayous, C. Langlois, T. Oikawa, C. Ricolleau, and A. Sacuto, Phys. Rev. B **73**, 113402 (2006).
[24]G. Celep, Ph.D. thesis, University Claude Bernard Lyon 1, 2006 .
[25]H. Portalès, L. Saviot, E. Duval, M. Fujii, S. Hayashi, N. Del Fatti, and F. Vallée, J. Chem. Phys. **115**, 3444 (2001).
[26]W. Reichardt, F. Gompf, M. Aïn, and B. M. Wanklyn, Zeitschrift für Physik B, Condensed Matter **81**, 19 (1990).
[27]M. M. Beg and S. M. Shapiro, Phys. Rev. B **13**, 1728 (1976).